Construction and Building Materials 379 (2023) 131225

Contents lists available at ScienceDirect

Construction and Building Materials

journal homepage: www.elsevier.com/locate/conbuildmat

Buckling capacity model for timber screws loaded in compression: Experimental, analytical and FE investigations

Angelo Aloisio [a,b,*], Yuri De Santis [a], Matteo Pelliciari [c], Marco Martino Rosso [d], Massimo Fragiacomo [a], Roberto Tomasi [b]

[a] Department of Civil Engineering, University of L'Aquila, Italy
[b] Faculty of Science and Technology, Norwegian University of Life Sciences, Norway
[c] Department of Engineering "Enzo Ferrari", Università degli Studi di Modena e Reggio Emilia, 41125 Modena, Italy
[d] Politecnico di Torino, DISEG, Department of Structural, Geotechnical and Building Engineering, Corso Duca Degli Abruzzi, 24, Turin 10128, Italy

ARTICLE INFO

Keywords:
Screws
Buckling
Timber
Compression perpendicular to grain
Experimental tests
Analytical model
FE validation

ABSTRACT

This paper investigates the buckling of screws loaded in compression inserted into timber members. Screws are often used as a reinforcement in timber structures. However, under compression forces, they are prone to axial buckling. The current model for the screw buckling, enclosed in the EC5 proposal, is based on the general framework of EC3 for the instability of compressed steel members. The main shortcomings of the current formulation for the buckling of screws are the following. (1) The analytical expression for calculating the theoretical buckling load does not follow the observed modes. (2) Due to the need for dedicated studies, the value of the imperfection coefficient is arbitrarily chosen. This paper fills the above gaps. Firstly, a simple analytical expression for predicting the buckling of screws is proposed and validated against experimental and finite element (FE) findings. Furthermore, the formulation adopts a more accurate expression for lateral deformation based on experimental observation. Secondly, a FE model calibrated on experimental tests is used to estimate the defect coefficients of the instability curves as a function of the amplitude of the geometric defects of the screw, expressed as a fraction of its length. Finally, a Markov chain Monte Carlo analysis is carried out to simulate the capacity of screws with different sizes, assuming the uncertainty of all input parameters sampled from suitable probability distributions. The results are used to validate the proposed deterministic capacity model and estimate the uncertainty factors of the design equation.

1. Introduction

The increasing importance of mass timber structures is also related to the development of self-tapping screws (STS) [5]. STS is growing as the leading fastener system in timber engineering, used in timber-to-timber [6–8], steel-to-timber [9] and concrete-to-timber [10]. An STS consists of three main components: the head (sunk or non-sunk), thread (full or partial) and self-drilling tip [11–13]. STS are often used as reinforcements to prevent failure mechanisms associated with compression perpendicular to the grain (CPG), shear stresses [10,14,15], or tensile stresses perpendicular to grain [7,11,16], see the screw reinforcement around holes in timber beam [17–19,19–22].

Mainly to avoid excessive local deformation, the screws can be used to reinforce timber members under CPG [12,23]. In this case, the screws are subjected to axial forces applied at the screw head. There are standard design approaches for timber under CPG, mainly originating from [24,25]. The standard capacity model for timber reinforced with screws is additive [26,27]. The capacity is the summation between the wood and screw resistance. The timber CPG strength has been extensively investigated since the early 1900 [28]. Conversely, less research was directed to the screw capacity characterization under axial force.

The screw capacity is estimated as the minimum between the push-in and buckling resistance. The push-in resistance is straightforward to evaluate since it can be estimated by multiplying the withdrawal strength by the screw surface. Besides, due to the symmetry between push-in and withdrawal behaviour, there are extensive experimental campaigns for its resistance and stiffness characterization: studies on withdrawals can be considered valid also for push-in. Conversely, the buckling model has never been investigated systematically.

* Corresponding author at: Department of Civil Engineering, University of L'Aquila, Italy.
E-mail addresses: angelo.aloisio1@univaq.it (A. Aloisio), yuri.desantis@univaq.it (Y. De Santis), matteo.pelliciari@unimore.it (M. Pelliciari), marco.rosso@polito.it (M.M. Rosso), massimo.fragiacomo@univaq.it (M. Fragiacomo), roberto.tomasi@nmbu.no (R. Tomasi).

https://doi.org/10.1016/j.conbuildmat.2023.131225
Received 11 January 2023; Received in revised form 22 March 2023; Accepted 27 March 2023
Available online 3 April 2023

List of symbols and notations

A	Area of the section of the screw.
A_{imp}	Amplitude of the geometric imperfection of the screw defined in Fig. 8.
a_1	Spacing between screw or rod reinforcement in the direction parallel to the grain.
a_{3c}	Distance between the screw closest to the member edge and the member end in the direction parallel to the grain.
α	Angle between screw axis and grain direction of the wood.
α_g	Imperfection coefficient in Eq. (3) defined for steel members in Table 4.
β	Constant appearing in Eq. (A.8) defined as $(c_v/EA)^{0.5}$.
b	Member width.
b_c	Width of the contact area for the reinforced member under compression perpendicular to the grain.
$c_h = (0.19 + 0.012d)\,\rho\left(\frac{90°+\alpha}{180}\right)$	Horizontal sub-grade coefficient for the screw for solid timber, glued laminated (GL) timber of softwood. c_h is in MPa if d is in mm, ρ in kg/m^3 and α in degrees.
$c_{v,exp} = 234\frac{(\rho d)^{0.2}}{l_w^{0.6}}$	Horizontal sub-grade coefficient for the screw for solid timber, glued laminated (GL) timber of softwood. c_v is in MPa if d is in mm, ρ_k in kg/m^3.
c_v	Horizontal sub-grade coefficient for the screw used in Eq. (A.8).
CoV	Coefficient of variation.
CPG	Compression perpendicular to the grain.
d	Outer thread diameter of the screw.
d_1	Inner thread diameter of the screw estimated as $0.5d$.
ϵ	Standard normal distribution.
E	Young's modulus of steel equal to 210 GPa (*).
F	Resistance of a timber member with screw reinforcement under compression perpendicular to the grain (*).
F_w	Withdrawal capacity of the screw (*).
f_w	Withdrawal strength of the screw (*).
F_c	Axial capacity of the screw (*).
$F_{fem,\mathrm{NLSIM}}$	Axial capacity of the screw from the FE model assuming an initial geometric imperfection (*).
F_{exp}	Experimental capacity of the screw estimated as the maximum of the experimental curve.
f_y	Yielding strength of the steel (*).
$f_{c,90}$	Compression strength perpendicular to the grain (*).
$k = 0.5\left[1 + 0.49\left(\bar{\lambda} - 0.2\right) + \bar{\lambda}^2\right]$	Buckling coefficient for the screws.
k_c	Proposed reduction coefficient of the yielding strength of the screw.
$\kappa_c = \begin{cases} 1, & \bar{\lambda} \le 0.2 \\ \frac{1}{k+\sqrt{k^2-\bar{\lambda}^2}}, & \bar{\lambda} > 0.2 \end{cases}$	Reduction factors for screw buckling. Alternatively, the values in Table 1 can be used. For values not included in Table 1 a linear interpolation should be carried out.
k_{pr}	Parameter adopted for screws in reinforced compression perpendicular to the grain (this parameter was originally indicated as $k_{c,90}$ in EN 1995-1-1). According to prEN1995-1-1, it considers the material behaviour and the degree of deformation perpendicular to the grain. The value of k_{pr} according to Blass [1] and the existing version of EN 1995-1-1 [2] can be assumed as 1,75 for glulam members on discrete supports loaded by distributed loads and/or by concentrated loads at a clear distance from the support larger or equal to $2h$, or 1,5 in case of glulam member on continuous support (sill configuration). For the other cases the value of k_{pr} can be assumed equal to 1.
k_p	According to prEN1995-1-1, it takes into account the material behaviour and the deformation perpendicular to the grain. The factor accounts for the increased stiffness when the deformation increases [3], see Table 2.
$k_w = \begin{cases} 1, & 30° \le \alpha \le 90° \\ 1 - 0.01(30° - \alpha), & 0° \le \alpha < 30° \end{cases}$	Parameter for screws and rods with wood-screw thread, where α is the angle between the fastener axis and the direction of the grain.
$k_{mat} = \begin{cases} 1.0, & n_p = 1 \\ 1.06, & n_p \ge 2 \\ 1.10, & n_p \ge 3 \\ 1.13, & n_p \ge 5 \\ 1.15, & n_p \ge 7 \end{cases}$	Material parameter for the number of laminations, where n_p is the number of laminations.
h	Height of the timber member.
I	Moment of inertia of the screw estimated as $(\pi d_1^4/64)$.

K_{ax}	Axial stiffness of the screw.
l	Total length of the screw.
l_c	Length of the contact area for the reinforced member under compression perpendicular to the grain.
l_r	Penetration part of the threaded part of the screw.
$l_{ef,1}$	Effective contact length parallel to the grain in correspondence of the contact area for a reinforced member under compression perpendicular to the grain.
$l_{ef,2}$	Effective distribution length parallel to the grain defined by the screw or rod types for a reinforced member under compression perpendicular to the grain.
$\bar{\lambda} = \frac{N_{pl}}{N_{ki}}$	Relative slenderness ratio of the screws (*).
m	Order of the sine function associated with the first buckling mode in Eq. (A.6)
n	Number of fully threaded screws.
n_0	Number of fully threaded screws or rods arranged in a row parallel to the grain.
N_{pl}	Characteristic yielding strength of the screw (*).
$N_{ki} = 2\sqrt{c_h EI}$	Approximate ideal elastic buckling of a Winkler beam (*).
N_w	Ideal elastic buckling of a Winkler beam, expressed by Eq. (A.5) (*).
N_p	Proposed theoretical elastic buckling of a Winkler beam, given by Eq. (17) (*).
$N_{fem,buck}$	Ideal elastic buckling of a screw estimated with the FE model (*).
ξ	Reciprocal of the fraction of the screw length which represents the geometric imperfection defined in Eq. (18).
ρ	Density of wood (*).
σ_h	Standard deviation of the empirical regression for c_h in Eq. (7) estimated from [4] and defined in Table 8.
σ_v	Standard deviation of the empirical regression for c_v in Eq. (A.12) estimated from [4] and defined in Table 8.
$u(x)$	Axial displacement of the screw as a function of the abscissa x.
$v(x)$	Transverse displacement of the screw as a function of the abscissa x.
γ_R	Partial factor for material property.
γ_{M1}	Partial factor for a design resistance based on a (semi) empirical analysis with a ductile failure mode.
(*)	The addition of a subscript k indicates the corresponding characteristic value.

Table 1
Reduction factors due to buckling, where α is the angle between screw axis and grain.

f_{yk} [Mpa]	$\alpha = 90$	$\alpha = 0$
1000	0.6	0.5
800	0.65	0.55
500	0.75	0.65

Table 2
Values for k_p from prEN 1995, valid for solid timber, glulam, and CLT.

Cases	Case A	Case B	Case C
Deformation	2.50%	10%	20%
k_p factor	1.4	2.1	2.7

The buckling model for the screws originates from the DIN [16] and corresponds to the general framework in the EC3 [29] for steel members loaded in compression. It evaluates the buckling load as the product between the plastic resistance and the buckling reduction factor, a function of the theoretical buckling load. Given the general framework for compression buckling, Bejtka [4] observed that the buckling load is difficult to obtain with a closed-forced analytical expression and complied tables for the buckling load based on FE analyses in Ansys. The current EC5 proposal acknowledges the difficulty of using tables or FE to calculate the theoretical buckling load. Therefore, it estimates the buckling using a simplified expression valid for beams embedded in an elastic subgrade under a constant axial force. Despite the severe limitations, approximations and inaccuracy of the model, the predictions agree with the experimental results. However, as later discussed, this agreement depends on the low sensitivity of the buckling model to the theoretical buckling load rather than on the reasonable acceptability of the inherent model assumptions.

No paper attempts to critically discuss the buckling model for screws based on FE or analytical investigations. Additionally, despite the considerable research in pile modelling, there has never been exchanging of knowledge between geotechnics and timber engineering. The review by Poulos and Davis [30] shows that the buckling studies on slender piles range from the 1929 analysis by Granholm [31], who used the Winkler foundation for representing the soil response, to more recent computer analysis, which uses the elastic continuum as a soil model. However, the main limitations of existing analytical models are that foundation is homogeneous, and the loading is concentrated at the extremities of the pile [32–34].

The analytical solutions proposed by Hetenyi [32] and Timoshenko and Gere [35] should not be considered valid for screws since the axial force is not constant and vanishes at the screw tip. Likewise, Terzaghi affirmed that, also in geotechnics, there are circumstances where the analytical solutions cannot be considered valid [36]. For piles, the primary source of inaccuracy is the uncertainty of the subgrade reaction characterization [37,38]. The error associated with a mistaken soil characterization can be considered more critical than the modelling error. Therefore, it is generally accepted that the Winkler model does provide a reasonably accurate method for estimating the lateral response of piles [34].Despite the general acceptance of the classical Winkler model [39], there is advanced research on pile stability accounting for a nonuniform axial force. For instance, Heelis [40] studied

the stability of piles supported vertically by a frictional force. Nonetheless, the intrinsic uncertainty of the soil characteristics makes it difficult to transfer knowledge from structural mechanics to geotechnical design [41].

Conversely, the subgrade reaction in the screws is known with higher accuracy than the soil [4]. Therefore, considerable research aimed to characterize the horizontal and vertical subgrade reactions in screws. The estimation of the vertical subgrade reaction is associated with studies on the withdrawal properties of STS. Initial investigations by Blass et al. [42] led to an empirical equation for predicting withdrawal stiffness as a function of the wood density, screw diameter and penetration length. The empirical model was later modified by Ringhofer et al. [43] based on more extensive testing, considering the influence of laminated timber products (e.g., GLT, CLT) and thread of the screws (e.g., fully and partially threaded). Recently, Stamatopoulos and Malo [44] developed a withdrawal stiffness equation that accounts for the influence of grain angle. Even with the above modifications [44], the model for the axial stiffness leads to less accurate results than models for the lateral stiffness. For instance, the model by Bejtka yielded an R^2 close to 0.6 for the axial stiffness.

Conversely, the horizontal subgrade reaction, embedment stiffness, can be predicted with higher accuracy [45,46]. Bejtka obtained an R^2 higher than 0.9 using simple empirical regression. The current Eurocode 5 [47] only provides the lateral stiffness for bolted connections expressed as a function of wood density and dowel diameter. However, the EC5 proposal encloses an expression for the lateral stiffness of the screws following. Bejtka [42]. Bejtka proposed an expression for predicting the embedment stiffness as a function of the wood density, screw diameter and insertion angle. The embedment and axial stiffness are needed for rigorous mechanics-based screw models [48]. Nonetheless, the above empirical regressions were mainly used to evaluate stiffness properties [49] rather than refining or analysing the buckling model of screws.

Given the satisfactory accuracy of the empirical regressions for the lateral and axial subgrade reaction, improving the current buckling model for screws is reasonable. Moreover, unlike geotechnics, the lower uncertainty of the embedment stiffness makes it worthwhile to reduce the modelling error. So far, the main obstacle against the development of the model was the lack of a free database of experimental tests on buckling screws, despite the numerous difficulties carried out in the past [50]. To the authors' knowledge, no paper attempts to reduce the modelling error for predicting the buckling of the screws using a rigorous mechanics-based formulation.

This paper provides a theoretical derivation of an analytical equation for estimating the buckling load of screws based on the observed buckling mode. Additionally, the authors use a FE model to calibrate the defect coefficients of the improved buckling capacity model as a function of the initial screw imperfection. The paper comprises four main parts: experimental tests (Section 3), analytical derivation (Section 4), FE model calibration (Section 5), and Monte Carlo simulations (Section 6). Section 2 explains the paper's methodology, introducing the reader to the following investigations. The section on experimental tests is reported before the analytical and FE models to give the reader a physical understanding of the buckling failure modes observed in actual screws. The observation of the buckling modes will be used to develop the analytical formulation for the instability problem.

The findings of this paper will need further validation by more extended experimental campaigns. The current experimental investigation comprises tests on eight screw types, each with two repetitions. Unfortunately, the exiguous number of tests is insufficient for adequately validating the proposed model due to the high variability in the mechanical response of screw connections. Nonetheless, despite this limitation, this paper hopefully paves the way to an alternative approach for modelling the buckling of screws under compression.

Table 3
Synoptic table on the standard model for the buckling capacity of timber screws.

Buckling resistance of the screws (prEN 1995-1-1)	
$F_c = k_c N_{pl}$	(1)
$\kappa_c = \begin{cases} 1, & \bar{\lambda} \le 0.2 \\ \frac{1}{k+\sqrt{k^2-\bar{\lambda}^2}}, & \bar{\lambda} > 0.2 \end{cases}$	(2)
$k = 0.5\left[1+\alpha_g\left(\bar{\lambda}-0.2\right)+\bar{\lambda}^2\right]$ where $\alpha_g = 0.49$; See Table 4	(3)
$\bar{\lambda} = \left(\frac{N_{pl}}{N_{ki}}\right)^{0.5}$	(4)
$N_{pl} = \pi \frac{d_1^2}{4} f_y$	(5)
$N_{ki} = 2\sqrt{c_h EI}$ [a]	(6)
$c_h = (0.19+0.012d)\,\rho\left(\frac{90°+\alpha}{180}\right)$	(7)

[a]See Appendix A for further details on the choice of N_{ki}.

2. Problem formulation and methodology

In 2012, the European Committee for Standardization (CEN) made a program to develop the second generation of Eurocodes, including new materials, products, and construction methods [51]. Eurocode 5 — design of timber structures, NS-EN 1995-1-1, includes a buckling model for screws. The working draft, prEN 1995 of November 2021, reports a set of equations for calculating the axial resistance of the screws, summarized in the synoptic Table 3. A detailed definition of the notation is given at the beginning of the paper.

The buckling model for timber screws under compression in Table 3 originates from the standard DIN 18800 [4] and coincides with the general formulation valid for axial buckling of steel members reported in the current EC3 [29,52]. Estimating the axial resistance requires the computation of two inputs, the theoretical buckling load and the plastic resistance, as shown in Fig. 1. The theoretical buckling load expresses the ideal buckling force without defects. At the same time, plastic resistance is the axial resistance of the element in the absence of instability phenomena. The ideal buckling never occurs due to initial imperfections, which reduce the theoretical buckling load. Therefore, the classical formulation assumes the resistance as the product between the plastic resistance and a buckling reduction coefficient, see Eq. (1). The buckling coefficient in Eq. (2) is different than one only for screws with relative slenderness higher than 0.2, where the slenderness in Eq. (4) is computed as the ratio between the plastic (Eq. (5)) and the ideal buckling force (Eq. (6)).

The model in Table 3 is not specific to the screws but comes from the traditional mathematical framework for instability phenomena. The model in Table 3 has been applied as it is to the screws with two modifications:

- Adopting Eq. (6) for estimating the ideal buckling load of the screws.
- Assuming a constant defect class c for the screws, with the corresponding defect coefficient equal to 0.49 [29].

The first assumption is incorrect since the solution in Eq. (6) has several limitations; the most relevant is the buckling mode. A simple sine is the buckling mode corresponding to Eq. (6) . However, experiments show that the buckling of the screw takes place with a concentration of the deformation close to the applied load. The deformation tends to vanish rapidly; thus, a simple sine is not appropriate to describe such buckled mode. All Eq. (6) assumptions are discussed in-depth in Appendix A. The following limitations of the buckling formulation are highlighted:

1. The deformed shape is a simple sine, which does not mirror the buckling mode of a screw inserted in an elastic medium. A damped sine is more appropriate, see Fig. 2.

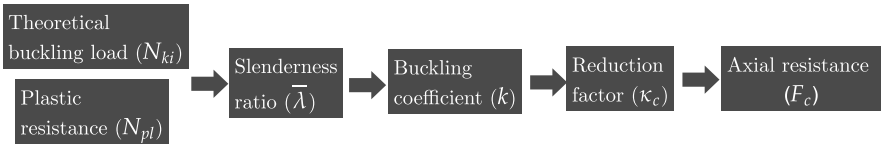

Fig. 1. Illustration of the steps needed for the computation of the compression resistance of timber screws.

Fig. 2. Buckling failure of a screw loaded in compression.

Table 4
Values of the geometric imperfection factor (α_g) for various stability curves.

Stability curve	a_0	a	b	c	d
α_g	0.13	0.21	0.34	0.49	0.76

2. Eq. (6) does not respect the boundary conditions for a pinned–pinned beam assumed in the formulation [35,53].
3. The axial force is assumed constant along the axis of the screw, and the axial stiffness is infinite.

Regarding the second aspect, no studies relate the screw defects to the imperfection coefficients. Additionally, the substantial difference between the buckling mode of steel members loaded in compression (a sine) and the screw (a damped sine) compromises the direct application of the imperfection coefficients of EC3 to the screws.

Therefore, the model in the synoptic Table 3 might need the twofold enhancements:

- An expression for the theoretical buckling load based on a suitable assumption for the buckling mode.
- Calibration of the geometric uncertainty factors (α_g), appearing in Eq. (3) as a function of the initial geometric imperfection. The EC5 proposal assumes $\alpha_g = 0.49$, corresponding to a class c in Table 4. However, this parameter has never been calibrated on the screws for different values of the initial geometric defect. Furthermore, the values in Table 4 cannot be directly used for the screws since the buckling mode of the screws is significantly different from a sine.

Given the above considerations, the objectives and novelties of this paper are the following:

- Theoretical derivation of an analytical equation for estimating the buckling load of screws based on the observed buckling mode.
- FE modelling of the tested configurations used to (i) validate the theoretical buckling load estimated using the proposed equation and (ii) calibrate the effect of the initial geometric defect on the capacity.

The research path followed in this paper is illustrated in Fig. 3. The problem is tackled by analysing and discussing experimental tests on screws loaded in compression. The analyses reveal the buckling modes and provide the actual capacity of the screws. The first step is deriving a theoretical formulation for the critical buckling load. The formulation is based on an assumption of the buckled shape from experimental evidence. The model is validated against the theoretical buckling loads obtained from the FE model. The second step deals with the FE investigation considering the effect of geometric defects. This step consists of three phases:

- Development of a linear FE model of the screws loaded in compression, representing the experimental configurations, for estimating the theoretical buckling loads and the related buckling modes. In this phase, the authors validate the analytical expression for the theoretical buckling and compare the experimental, FE and analytical predictions for the buckling modes.
- Calibration of the geometric defect of the screws using the experimental data. The axial capacity is obtained from a quasi-static nonlinear push-in analysis of the screws, assuming an initially deformed configuration corresponding to the first buckling mode, estimated from the solution of the linear instability problem. In this phase, the authors compare the FE predictions for the axial capacity and the corresponding experimental values.
- Markov chain Monte Carlo (MCMC) analyses [54] of the push-in FE simulations assuming the uncertainties of all input parameters obtained by sampling suitable probability distributions, given different values for the initial geometric imperfection. This section aims to estimate the geometric uncertainty factor in Eq. (3) given different amplitudes for the initial geometric imperfection, expressed as a fraction of the screw length. Additionally, the MCMC analyses lead to an estimate of the uncertainty safety factors of the corresponding design equations. Finally, it must be remarked that for the first time, the values for α_g are estimated for timber screws.

3. Experimental tests

The authors conducted compression tests on a set of timber screws used for validating the FE model of the screw and understanding the physics behind the buckling of the screws. The screw has been directly loaded by connecting a Torx bit to the load cell through a steel plate. The steel plate and Torx bit used for the tests are shown in Fig. 5. The test specimens are glue-laminated timber of strength class GL30c (ρ_k = 390 kg/m^3, ρ = 430 kg/m^3), with dimensions of 800 × 140 × 225 or 1200 × 140 × 540 mm (length × width × height). Rothoblaas produced the screws. The mean moisture content of the specimens measured by a Delmhorts RDM3 instrument was 12.3%. Fig. 4 shows a schematic overview of the different screws, reporting the effective screw length (l_r) applied in the design model. The column named "Head" describes the geometry of the screw head. The predicted failure mode is according to the design model.

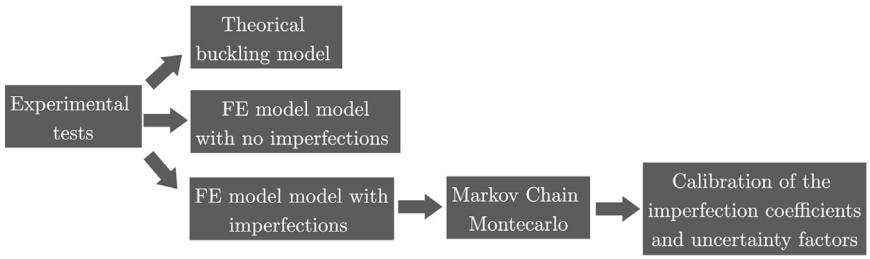

Fig. 3. Workflow of the investigation carried out in this paper.

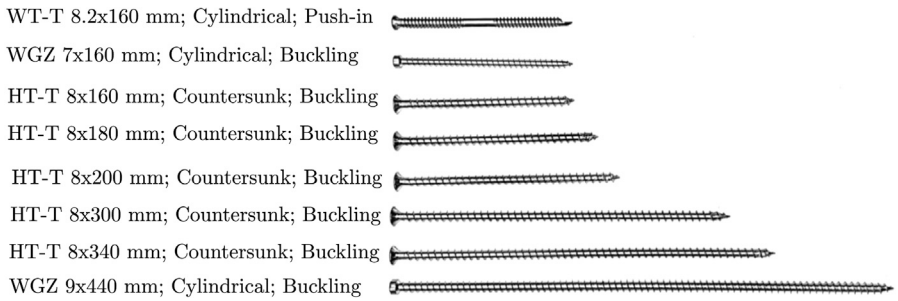

Fig. 4. View of the tested screws. The first label indicates the screw type, followed by the geometry (diameter × length), the head type and the predicted failure mode.

Fig. 5. Setup of specimen with height 540 mm in ZwickRoell Z1200-Steel plate used for Torx tests — Setup of Torx test.

The screws are fully threaded self-tapping screws, except for the WT-T screw, which is double-threaded and has a threaded length equal to 130 mm. They were drilled with a right angle, and the head was flushed in the timber surface. The screw is compressed using a load cell of the ZwickRoell Z1200 UTM (Universal Testing Machine).

The loading protocol detailed in [12] consists of three phases following EN408 and ISO6891. Phases 1 and 2 follow ISO6891 to avoid initial residual deformations and stabilize the loading area. The specimen is loaded up to 40% of the estimated resistance (F_c), held for 30 s before the load decreases to 10% of F_c, and then held for 30 s. The load rate in phases 1 and 2 is determined as the ratio between 40% and 10% of F_c respectively, and 60 s. The actual load–displacement curves used in the analyses correspond to phase 3. Phase 3 follows EN408. Hence, the maximum force will be reached within 300 ± 120 s.

The authors carried out sixteen tests, eight configurations and each with two repetitions. Fig. 6 displays the force–displacement curves. The capacity is estimated from the maximum of the curve; see Fig. 6(b). The trend is almost linear up to the attainment of the resistance. Then, there is a sudden, nearly vertical drop due to the achievement of the buckling load.

Six out of the eight screws failed due to axial instability; see Fig. 7 showing typical buckling modes. Table 5 reports the experimental and predicted capacity using Eq. (1). The discrepancies between the predictions and the estimates are:

- The failure mode is always buckling, except for the short screws VGZ 7.0 × 160 and WT-T 8.2 × 160.
- The relative error between the predictions using Eq. (1) and the experimental values is higher than 100%. Although this difference might appear irrelevant for a single screw in absolute values, it might be more significant when dealing with reinforcements using multiple screws.

The deformation of the buckling mode is localized at the screw head. The head almost remains aligned with the screw axis. Right after the head, the screw exhibits a single bend, while the remaining part of the screw is almost undeformed. The shape of the buckling mode mainly depends on the stress localization at the screw head, as discussed in the appendix (see Eq. (A.11)). The observed buckling mode is far different from that assumed in the estimation of Eq. (6) , corresponding to a simple sine [35].

The authors tested 5 HT-T screws with different lengths. According to Eq. (6) , the length of the screw does not affect the buckling capacity. Still, the experimental data reveal experimental capacities ranging from nearly 25 to 29 kN. This is an approximate 10% relative variation,

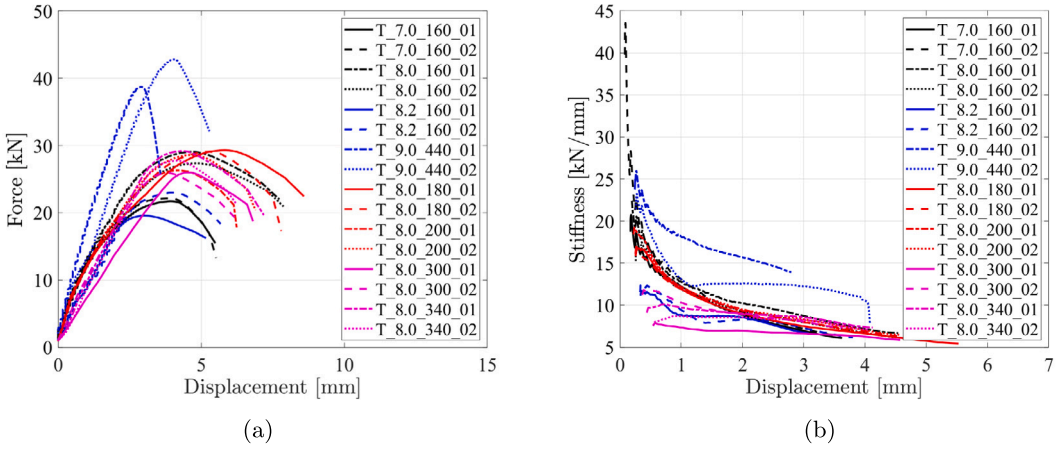

Fig. 6. Load–displacement (a) and Stiffness–displacement (b) curves.

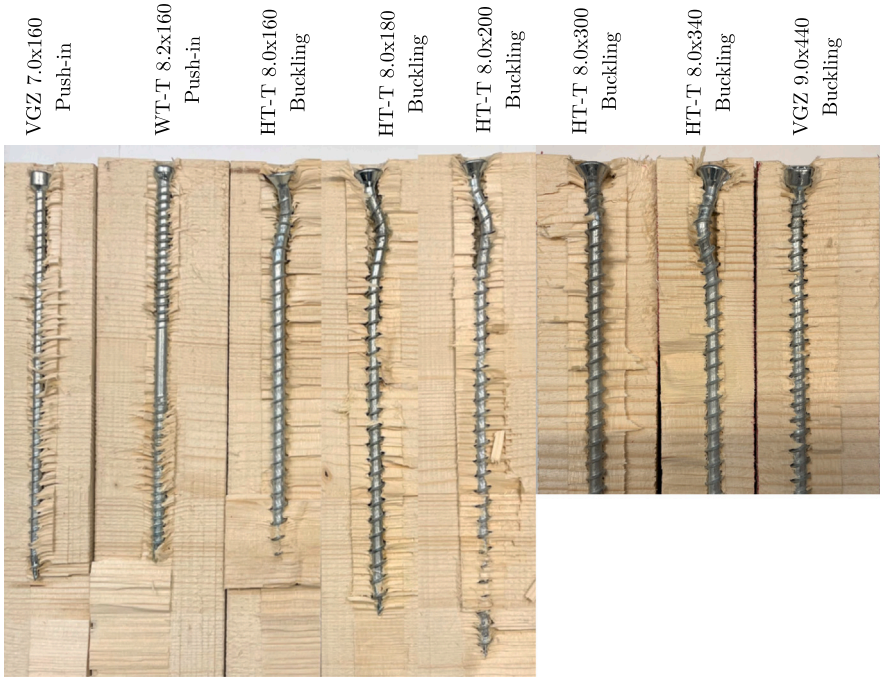

Fig. 7. Failure modes of the tested screws.

Table 5
Comparison between experimental and predicted capacity, where $F_{exp,1}$ and $F_{exp,2}$ are the experimental capacities of the first and second test repetition, F_{exp} is the mean between $F_{max,1}$ and $F_{exp,2}$, F_c is the predicted value according to EC5 in kN based on Table 3.

Screw type	d [mm]	l_r [mm]	$F_{exp,1}$	$F_{exp,2}$	F_{exp}	F_c Eq. (1)	Error [%]	Exp. Fail.	Pred. Fail.
VGZ	7	160	21.7	22.1	21.9	9.7	126.6%	Push in	Buckling
WT-T	8.2	130	19.6	23.0	21.3	13.4	58.9%	Push in	Buckling
HT-T	8	160	29.1	27.4	28.2	12.7	121.6%	Buckling	Push in
HT-T	8	180	29.3	29.1	29.2	12.7	129.3%	Buckling	Buckling
HT-T	8	200	26.3	28.6	27.5	12.7	115.7%	Buckling	Buckling
HT-T	8	300	26.0	25.9	26.0	12.7	103.9%	Buckling	Buckling
HT-T	8	340	29.2	27.8	28.5	12.7	123.8%	Buckling	Buckling
VGZ	9	440	38.7	42.8	40.8	16.2	151.3%	Buckling	Buckling

which can be considered coherent with the non-dependency of F_c on the screw length. Additionally, the variation of the experimental capacity is not correlated to the screw length. In some cases, the shortest and the longest screws, 180 mm and 340 mm, have the same capacity, which is 29 kN. This fact proves that the observed scatter of the HT-T screws depends on the aleatoric uncertainty associated with the experimental test repetition.

4. Proposed theoretical formulation for the critical buckling load

As previously mentioned, the classical solution to the buckling problem of a bar on an elastic foundation is derived by assuming a simple sine as buckled shape. However, the experiments show that the actual deformed shape exhibits a sinusoidal trend close to the loaded end of the screw. Right after, the deflection smoothly decreases. Thus,

assuming a damped sine for the buckled shape seems more appropriate. This assumption will be adopted in the following to propose a more accurate theoretical solution for the buckling of screws.

The solution to the buckling problem of a bar on an elastic foundation is derived under the following hypotheses: (i) the bar has an infinite axial stiffness; (ii) the ends of the bar are hinged; (iii) the variation of axial load along the longitudinal axis is neglected. Comments on this last hypothesis are given in Appendix A.2. Following the energy method, the critical value of the load can be found by minimizing the deformation energy [35], namely

$$\Delta U = \Delta T \tag{8}$$

where ΔU is the strain energy and ΔT is the external work.

The theoretical buckling load of a Winkler beam, expressed by Eq. (6) , was derived by assuming the following buckled shape [35]:

$$v(x) = c \sin\left(\frac{m\pi x}{l_r}\right) \tag{9}$$

In light of the previous considerations, a simple sine is not suitable for describing the actual buckled shape of the bar. Hence, a damped sine is adopted

$$v(x) = c\, e^{-\frac{m}{l_r}x} \sin\left(\frac{m\pi x}{l_r}\right) \tag{10}$$

The strain energy of the buckled bar is the sum of the energy associated with the bending and the subgrade deformation:

$$\Delta U = \Delta U_1 + \Delta U_2 \tag{11}$$

where

$$\Delta U_1 = \frac{EI}{2}\int_0^{l_r} v''(x)^2 dx = \frac{EI\left(5+\pi^2\right)\pi^2 c^2 e^{-m} m^3 \sinh(m)}{4{l_r}^3} \tag{12}$$

The lateral reaction of an element dx of the bar is $c_h v dx$. Hence, the total strain energy of the elastic medium is

$$\Delta U_2 = \frac{c_h}{2}\int_0^{l_r} v^2(x) dx = \frac{c_h \pi^2 c^2 l_r\, e^{-m}\sinh(m)}{2\left(2\pi^2 m + 2m\right)} \tag{13}$$

The work done by the axial force in the critical configuration is

$$\Delta T = \frac{N_{cr}}{2}\int_0^{l_r} v'(x)^2 dx = \frac{N_{cr}\pi^2 c^2 e^{-m} m \sinh(m)}{4 l_r} \tag{14}$$

Using Eq. (A.2), the following expression for the buckling load is obtained:

$$N_{cr} = \frac{c_h {l_r}^4 + \left(5+6\pi^2+\pi^4\right) EI m^4}{\left(1+\pi^2\right){l_r}^2 m^2} \tag{15}$$

The m value associated with the minimum of Eq. (15), provides the first critical load:

$$m_{min} = \left(\frac{c_h}{EI}\right)^{1/4} \frac{l_r}{\left(5+6\pi^2+\pi^4\right)^{1/4}} \tag{16}$$

By substitution into Eq. (15), the expression for the first buckling load N_p proposed in this paper is

$$N_p = 2\sqrt{c_h EI}\,\frac{\sqrt{5+6\pi^2+\pi^4}}{1+\pi^2} \approx 1.17 N_{ki} \tag{17}$$

Interestingly, N_p is 1.17 times the critical load N_{ki} obtained with the classical formulation. The following section will validate this result using FE analyses, showing that N_{ki} underestimates the critical load by, on average, 22%, while N_p provides a more accurate prediction.

It is worth noting that m should be a natural number. However, in general, the solution of Eq. (16) gives a real number. Nevertheless, as explained in Appendix A.1, this does not affect the solution sensibly, and the critical buckling load estimation is relatively accurate.

5. FE analyses

The authors developed a monodimensional FE model of the screw in Abaqus. Initially, the model validates the expressions for the theoretical buckling loads derived in the previous section. In a second step, the authors modified the model to include the effects of initial geometric imperfection, calibrated on the experimental data.

5.1. Model description and methodology

Two different finite element models have been developed. The first model is defined to validate the analytical formulations for the instability of screws, whilst the latter aims at describing the system's non-linear behaviour until failure.

In the linear buckling model (LBM) shown in Fig. 8(a), shear-deformable beam elements with linear interpolation represent the screw. This formulation considers the shear strain effects due to the cross-section not necessarily being normal to the screw axis.

The screw section is assumed to circular with diameter $d = 1.1 d_1$. A linear elastic constitutive model is adopted for steel ($E = 210\,000$ N/mm^2). Two orders of elastic spring elements describe the screw-timber interaction in the axial and transversal directions. Axial and transversal connectors stiffness are assumed as $C_v = c_v l_m$, and $C_h = c_h l_m$ respectively, where l_m is the length of the beam element between two adjoining connectors and c_v and c_h are determined according to Eqs. (A.12) and (7), respectively. The screw-head is assumed free to rotate and to translate in the screw axial direction while the transversal displacement is restrained. The load $\bar{F}$ is applied to the head-side end node as a concentrated force. The eigenvalues analysis is conducted in the initial undeformed and imperfection-free geometry. Differently from Bejtka [4], the screw head is considered pinned.

The non-linear static incremental model (NLSIM) in Fig. 8(b) assumes an elastic–plastic constitutive law for the steel, whilst an elastic behaviour is considered for both axial and transversal springs. In this way, the model can only predict the screw bending failure mode while neglecting the push-in failure mode, which is outside this research's scope. An imposed displacement $\bar{u}$ is applied to the head-side end node. A static-incremental geometrically and mechanically non-linear analysis is carried out on a defected screw geometry. As the initial screw geometrical imperfection shapes, the first buckling mode from LBM has been adopted (Fig. 8(b)) [55]. The amplitude A_{imp} is calibrated on the experimental results.

5.2. Theoretical buckling validation

The formulation in Eq. (17) is validated against the theoretical buckling loads obtained from the FE model. Table 6 compares the theoretical buckling load estimated with the LBM ($N_{fem,buck}$) with N_{ki} in Eq. (6) and N_p in Eq. (17).

The experimental capacities (F_{exp}) are not reference values for validating the accuracy of the theoretical buckling load predictions and thus are not reported in Table 6. The reference values, assumed as ideal buckling loads, are the FE predictions in $N_{fem,buck}$. Despite the straightforwardness of the proposed formulation, the mean error associated with N_p in Eq. (17) is approximately 9%. Conversely, the mean error of N_{ki} is approximately 22%.

The proposed buckling load, N_p, gives a better prediction than N_{ki} because it is derived by assuming a damped sine as a buckled shape instead of a simple sine. Furthermore, a damped sine can approximate the deformed shapes of both linear buckling and nonlinear incremental FEM analyses (see Figs. 8 and 10). The actual deformed shape from FEM analyses depends on both the geometrical and mechanical characteristics of the screw considered. A damped sine does not give a perfect characterization, but undoubtedly better than a simple sine. Yet, a very accurate buckling load prediction is hardly obtained from closed-form solutions. Nevertheless, the proposed formula for N_p gives

Table 6
Validation of the theoretical buckling load estimated with the FE model ($N_{fem,buck}$), compared against the theoretical buckling loads corresponding to the Winkler beam (N_{ki}) in Eq. (6) and the proposed Eq. (17) (N_p). The input parameters are $\rho = 430$ kg/m^3, $\alpha = 90°$, $d_1 = 0.65d$, $E = 210$ GPa. The diameter assumed in the calculations is $1.1d_1$.

Label	l_r [mm]	d_1 [mm]	c_h [MPa]	c_v [Mpa]	N_{ki} [kN]	N_p [kN]	$N_{fem,buck}$ [kN]
VGZ	160.0	5.0	117.8	55.3	55.2	64.6	73.0
WT-T	130.0	5.9	124.0	64.6	77.7	90.9	109.7
HT-T	160.0	5.7	123.0	56.8	73.7	86.2	99.5
HT-T	180.0	5.7	123.0	52.9	73.7	86.2	97.3
HT-T	200.0	5.7	123.0	49.6	73.7	86.2	95.6
HT-T	200.0	5.7	123.0	49.6	73.7	86.2	90.6
HT-T	300.0	5.7	123.0	38.9	73.7	86.2	89.4
VGZ	440.0	6.4	128.1	31.7	95.2	111.3	113.7
				Relative error	−0.22	−0.09	

Table 7
Finite element model (NLSIM) vs experimental results. The input parameters are $\rho = 430$, $f_y = 1200$, $\alpha = 90°$, $d_1 = 0.65d$, $E = 210$ GPa and $A_{imp} = l/500$. The diameter assumed in the calculations is $1.1d_1$.

Configuration	$F_{fem,NLSIM}$ [kN]	F_{exp} [kN]	Relative error [%]
T-7.0-160[a]	23.3	21.9	6.4
T-8.2-160[a]	32.3	21.3	51.9
T-8.0–160	30.7	28.2	9.0
T-8.0–180	30.5	29.2	4.6
T-8.0–200	30.3	27.5	10.4
T-8.0–300	29.2	26.0	12.5
T-8.0–340	28.8	28.5	1.2
T-9.0–440	35.9	40.8	−11.8

[a]Experimental push-in failure

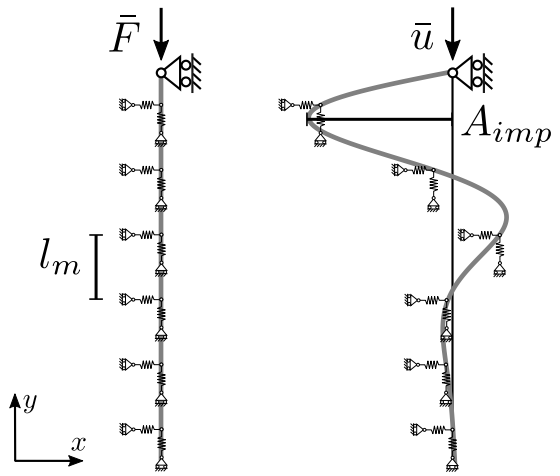

Fig. 8. Finite element models: (a) Linear buckling analysis and (b) Non-linear static incremental analysis.

a good prediction while maintaining an agile and explicit mathematical expression.

It must be remarked that the error associated with N_{ki} can be considered reasonable in some applications (like geotechnics), where the uncertainty of the soil properties are far more relevant than the modelling assumptions in Eq. (6) . However, the higher accuracy of Eq. (17) endorses its use in place of N_{ki} for predicting the ideal buckling of the screws, where c_h can be estimated with reasonable accuracy.

5.3. Calibration of the geometric defects

Initial imperfections and second-order effects affect the failure load of a beam loaded in compression on an elastic medium. The capacity of a perfectly straight beam made of an elastic–plastic material equals its plastic axial force $N_{pl} = f_y \pi d^2/4$. When initial imperfections occur, a bending moment arises in the beam as the beam deforms. Accordingly, the eccentricity between the load and the beam axis increases. The failure of the systems occurs for a combination of axial force and bending moment. Therefore the yielding tensile stress f_y and the initial imperfection amplitude A_{imp} directly influences the ultimate compression load of the screw. However, the failed configuration corresponds to the buckling mode, as occurs in all instability phenomena [55]. For this reason, it is necessary to know the ideal instability phenomena.

In the NLSIM, f_y equals the mean value of the tensile failure stress of the tested screws ($f_y = 1200$ N/mm^2). At the same time, the imperfection amplitude is calibrated on experimental results. The imperfection amplitude A_{imp} is defined as a fraction of the screw length following the general approach for steel structures [52]:

$$A_{imp} = l/\xi \tag{18}$$

The value of ξ has been determined by minimizing the sum of the squared relative error between NLSIM and the experimental results of the configurations that exhibited bending failure mode (Fig. 7):

$$S = \sum_{n=3}^{8} \left(\frac{F_{fem,NLSIM} - F_{exp}}{F_{exp}} \right)^2 \tag{19}$$

Fig. 9 shows the NLSIM failure load for increasing eccentricity values. The value of the objective function S is minimized when $\xi = 500$. The plot in Fig. 9 highlights the significant role of the geometric imperfections. In the case of low imperfections, the predicted capacity almost corresponds to the plastic capacity in Eq. (5). An increasing value of the imperfection significantly reduces the axial capacity and exalts the effects of instability. In the tested configurations, the estimated imperfection, equal to l/500, is very low compared to steel structures where the lowest imperfection class a_0 almost corresponds to an eccentricity equal to l/350 [52]. However, the two scenarios, the screw and the steel member loaded in compression are not comparable due to the mentioned differences in the buckling modes. Therefore, as discussed in the previous sections, the screws deserve a dedicated calibration of the imperfection coefficients in Eq. (3) and Table 4.

Fig. 9(b) displays the force–displacement curves of the updated model with $A_{imp} = l/500$, while the deformed shapes at failure and the bending moment contour are displayed in Fig. 9.

Table 7 compares the experimental vs FE estimations of the capacity using the optimized value for A_{imp} equal to l/500. The relative error is minimum and generally less than 10% except for the screw T-8.2–160. The finite element model can only predict the buckling failure mode, not the push-in one. Therefore, the FEM-predicted failure loads of T-8.2-160 and T-7.0-160 are not directly comparable to the experimental outcomes of push-in failure.

It is worth noting that the bending moment maxima approximately manifest at the same distance from the screw head for all configurations (≈15–20 mm). This result is confirmed by the experimental evidence in Fig. 7. The obtained value for the imperfection coefficient could be considered low due to the carefulness carried out in the screw drilling using a template for a right-angle insertion. Additionally, as shown in Fig. 7, no defects could have deviated from the screw during the drilling, thus causing a straightness defect.

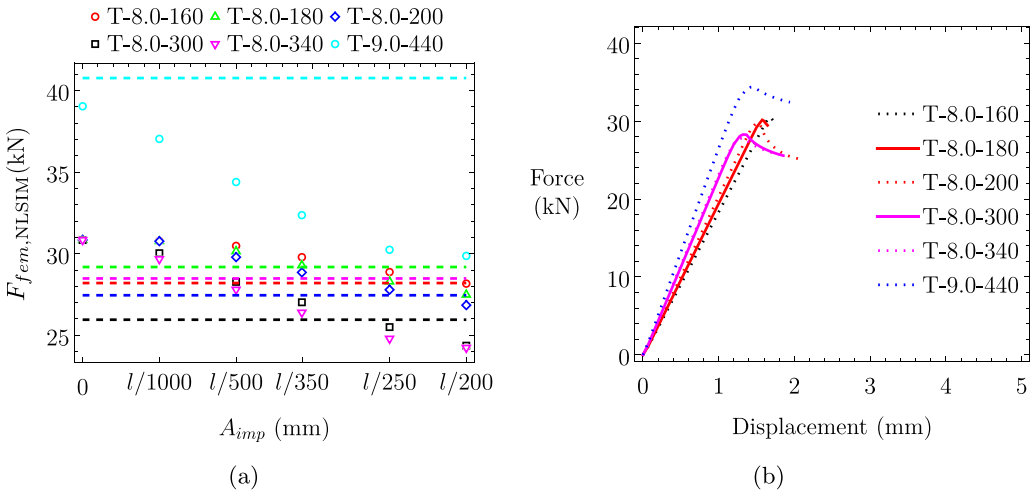

Fig. 9. (a) Finite element predicted failure loads (markers) and experimental failure loads (dashed lines) for varying imperfection amplitude. (b) Finite element force–displacement curves with $A_{imp} = l/500$.

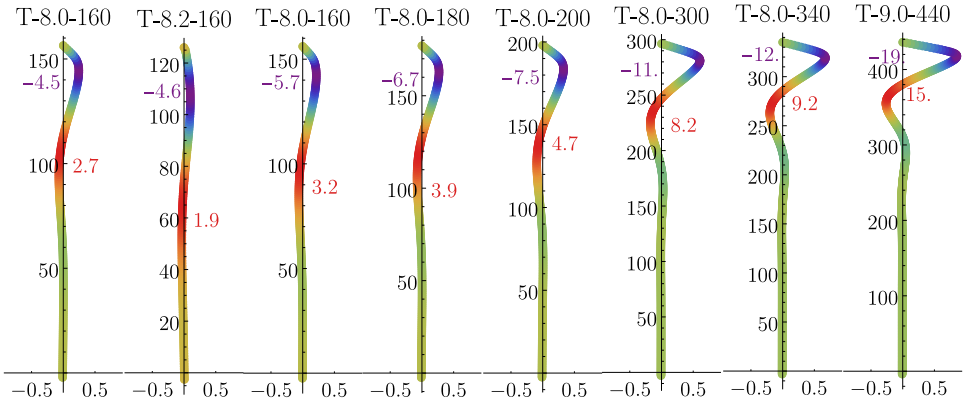

Fig. 10. Finite element predicted deformed shape at failure and bending moment contour (kNmm).

6. Monte Carlo simulations and imperfection coefficient calibration

The experimental results and analytical findings suggest two improvements to the model in Eq. (21):

- Replacing N_{ki} with N_p in Eq. (17).
- Adopting an imperfection coefficient (α_g) calibrated for different values of the geometric uncertainty (A_{imp}). This value depends on the laminated timber product, the distribution of defects, and the human error in screw insertion. This value should be decided on a case-by-case basis.

The authors carried out a Markov chain Monte Carlo analysis [54] to simulate the capacity of the screws with various lengths and diameters, assuming the uncertainty of the material inputs, as reported in Table 8.

Markov chain Monte Carlo (MCMC) methods comprise a class of algorithms for sampling from a probability distribution. This paper uses the Metropolis–Hastings algorithm to get a sequence of random samples from a probability distribution.

The diameter (d) has been randomly sampled from a uniform distribution with bounds in Table 8. The threaded length of the screw was obtained by inverting the equation for the withdrawal resistance, assuming the withdrawal resistance was normally distributed. Likewise, the yielding strength and the wood density are normally distributed following [42,56,57]. The scientific literature does not report the uncertainties associated with the empirical regressions for c_h and c_v. Bejtka only reports the coefficient of determination of the fitting for c_h and c_v. Therefore, the authors digitally converted the regression plots in the doctoral thesis from Bejtka [4] to estimate the fitting error. The histogram plot of the error follows a normal distribution with nearly-zero mean and variances reported in Table 8. Therefore, the authors included the uncertainty of c_h and c_v from a random sampling of the standard normal distribution (ϵ).

The authors repeated the MCMC for four values of imperfection: l/500, l/400, l/300, l/200, l/100 and l/50. Fig. 11 shows the histogram plots of the sampled values for f_y, ρ, d and the threaded length of the screw. Fig. 12 shows the superposition between the deterministic estimations of c_h and c_v and those with uncertainty based on Table 8. The c_h and c_v realizations have overlapped with the results reported by Bejtka for further validation of the proposed approach. The scatter of the data is very close to the one in the plots of Bejtka. The convergence of the Monte Carlo simulations was checked a posteriori from the CoV

Table 8
Input parameters of the Monte Carlo simulations.

Symbol	Distribution	Characteristics	
d [mm]	Uniform	Lower Bound = 1	Upper Bound = 20
l_r [mm]	$l = [\pi(d/2)^2 f_y]/(f_{ax} d)$		
ρ [kg/m^3]	Normal	μ = 470	CoV = 0.1 [42]
E [GPa]	Normal	μ = 210	CoV = 0.05 [42,56–58]
f_y [MPa]	Normal	μ = 1200	CoV = 0.05 [42,56,57]
f_w [MPa]	Normal	μ = 15	CoV = 0.1 [42]
c_h [MPa]	Eq. (7) $+\sigma_h \epsilon$	σ_h = 19.58	$\epsilon \propto \mathcal{N}(0,1)$ [4]
c_v [MPa]	Eq. (A.12) $+\sigma_v \epsilon$	σ_v = 14.86	$\epsilon \propto \mathcal{N}(0,1)$[4]

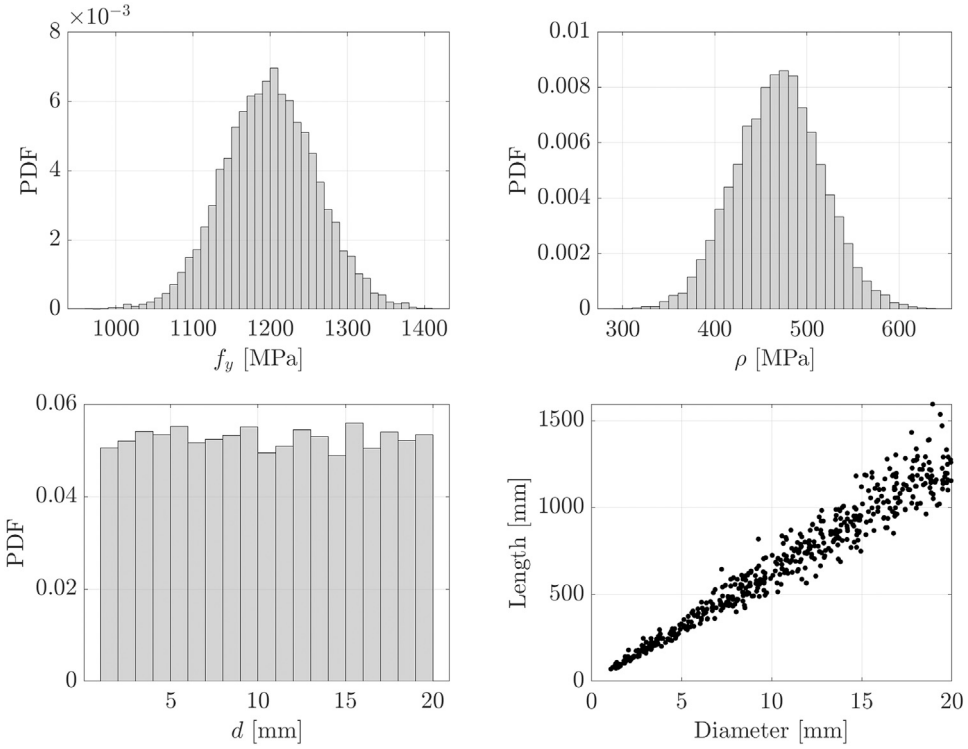

Fig. 11. Plots of the realization of the input parameters for the Monte Carlo analyses: (a) yielding strength, (b) wood density, (c) diameter, (d) threaded length of the screw.

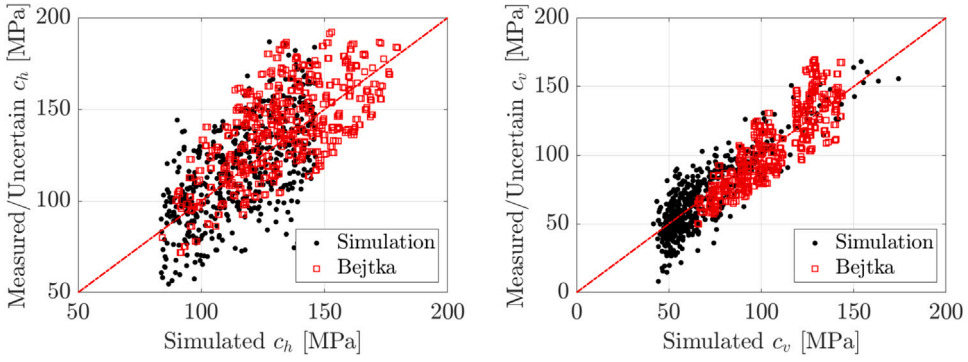

Fig. 12. In black the experimental/simulated values of c_h and c_v using the inputs in Table 8 vs the deterministic predictions using Eqs. (7) and (A.12), respectively. In red the experimental vs predicted values from Bejtka [4].

of the axial capacity. The analyses were stopped at 500 simulations since the variation of the CoV was less than 1%, as shown in Fig. 13. The values of α_g for the different geometric defects are obtained by minimizing the following objective function:

$$\hat{\alpha}_g = \arg\min_{\alpha_g \in \Omega} \left\{ \left[F_c - F_{fem,\mathrm{NLSIM}}(A_{imp}) \right]^2 \right\} \tag{20}$$

where $\Omega \in \mathrm{R}$, F_c is the buckling model in Eq. (1) where Eq. (17) is used for assessing the ideal buckling force and α_g in Eq. (3) is unknown. At the same time, $F_{fem,\mathrm{NLSIM}}$ is the capacity predicted by the FE model function of the initial geometric imperfection (A_{imp}).

Table 9 reports the values of the obtained imperfection coefficients by minimizing Eq. (20) using N_p for the ideal buckling load.

As expected, an increment of the imperfection level determines an increment of the corresponding imperfection coefficient α_g, see the stability curves in Fig. 14.

Fig. 15(a) shows the FE predictions of the theoretical buckling load vs the estimations using Eq. (6) (N_{ki}) and Eq. (17) (N_p). Additionally, Fig. 15(a) displays the FE predictions of the axial capacity vs the estimations of Eq. (5) with N_p and the imperfection coefficients in Table 9.

Table 9
Values of the calibrated imperfection coefficient $\hat{\alpha}_g$ as a function of the initial imperfection expressed as a fraction of the screw length. The ideal buckling load is estimated with Eq. (17).

$\hat{\alpha}_g$	l/500	l/400	l/300	l/200	l/100
	0.16	0.21	0.27	0.34	0.72

Table 10 reports the error of the three models F_c, N_p and N_{ki} in terms of mean error, standard deviation (SD), mean squared error (MSE), maximum Absolute Error (MAE), root Mean Squared Error (RMSE), and coefficient of determination (R^2), considering all defect scenarios.

The main findings of the analyses can be grouped into the following considerations:

- The theoretical buckling model which best fits the FE buckling predictions is the one in Eq. (17), despite the considered

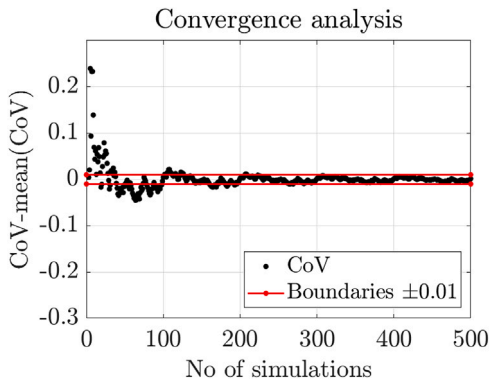

Fig. 13. Convergence of the Monte Carlo analyses regarding Coefficient of covariance (CoV).

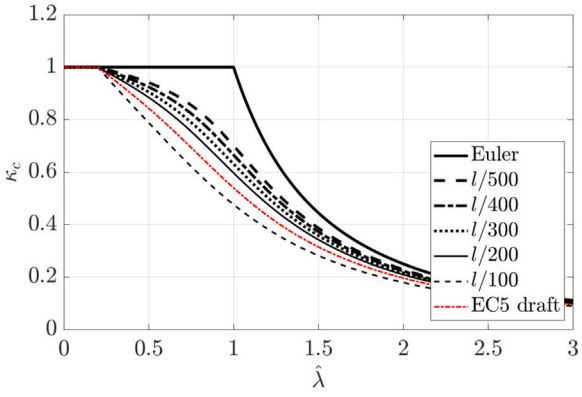

Fig. 14. Stability curves based obtained with the imperfection coefficients in Table 4.

Table 10
Mean error, standard deviation (SD) and mean squared error (MSE), Maximum Absolute Error (MAE), Root Mean Squared Error (RMSE) or the difference between the FE and analytically predicted force values (F_c), shown in Fig. 15. R^2 is the coefficient of determination of the fitting.

Model	Mean	SD	MSE	R^2	MAE	RMSE
F_c	−0.56	4.15	17.34	0.95	15.36	4.16
N_p	13.71	28.48	991.19	0.60	127.71	31.48
N_{ki}	−20.73	27.94	1202.71	0.56	114.30	34.68

uncertainties have a significant effect on the error metrics in Table 10. The differences between the predictions with N_p or N_{ki} are not significant in the presence of uncertainty. However, given the better performance of N_p and the more solid mechanical background, N_p should be preferred to N_{ki}.

- The axial capacity models obtained using Eq. (17) (N_p) and the imperfection coefficients in Table 10 are excellent. Therefore, despite the considered uncertainties of the FE model, the deterministic assessment of the capacity using the averaged values for the parameters in Table 8 is extremely accurate, with excellent error metrics in all configurations.

In conclusion, the prediction of the axial capacity of the screw in case of buckling can be carried out using Eq. (17) (N_p), where α_g is taken from Table 4. The main limitation of this paper is the lack of an extended experimental campaign relating the effects of geometric defects of the screw to the screw itself, the laminated timber product, the strength class (the density of defects), the timber species, etc. Therefore, future research efforts will aim at quantifying the influence of defects on the capacity estimate of the screws from experimental investigations.

Design codes require estimating the characteristic value, which can be obtained by replacing all mean values involved in the computation with the characteristic ones corresponding to a 5% fractile. Additionally, the potential use of the formulation requires the definition of an uncertainty factor γ_M to avoid underestimating the capacity due to the uncertainties involved. The code-format design capacity in Eq. (21) can be written as

$$F_{c,k} = \frac{1}{\gamma_M} k_c N_{pl,k} \tag{21}$$

The uncertainty factor γ_M is estimated by assuming that the design value is less than the corresponding experimental value with a probability equal to p as

$$P\left[F_c < F_{fem,\mathrm{NLSIM}}\right] = p \tag{22}$$

where F_c and F_{fem} are the simulated and experimental capacity corresponding to 1% deformation respectively, and p depends on the assumed reliability threshold. The European building code sets p as $\Phi(\alpha_R \beta_{LS})$, where $\Phi(\cdot)$ is the standard Normal cumulative distribution function, α_R is the sensitivity factor for the capacity, and β_{LS} is the safety index relevant to the considered limit state. Assuming a 50-years reference period for serviceability limit states (see Tab. C2 in Eurocode 0), $\beta_{LS} = 1.5$. The obtained γ_M coefficients corresponding to $\beta = 1.5$ range from 1.2 to 1.3. An increased defect causes a slight worsening of the predictions. The uncertainty factors slightly increase from an l/500 to an l/100 defect amplitude. Nonetheless, given the slight variation, the most conservative value, 1.3, is recommended for designing screws under compression loads.

7. Conclusions

This paper proposes a novel buckling model for timber screws based on the general mathematical framework for the instability of compressed steel members. The main shortcomings of the existing buckling model for the screws enclosed in the current Eurocode 5 draft are two: (1) the ideal buckling load is underestimated due to an incorrect assumption on the buckling shape; (2) the imperfection coefficients valid for compressed steel members exhibiting a sine-like buckling mode cannot be considered valid for timber screws loaded at one end.

The experimental and FE investigations showed that the buckling mode of the screws loaded at their heads resembles a damped sine function. As a result, the deformation of a buckled screw is concentrated at the load application point, while the remaining part of the screw is almost undeformed. Based on this evidence, the authors derived the critical buckling load of the screws assuming a deformation field having the shape of the observed failure modes. The error of the obtained formulation validated against the FE predictions is approximately equal to 9%. The proposed formulation is concise and corresponds to the classical one for the instability of Winkler beams multiplied by 1.17.

The proposed equation for the ideal buckling is used for calibrating the imperfection coefficients, assuming the mechanical parameters' uncertainty from suitable probability distributions and increasing levels of geometric imperfections of the screws. The authors estimated the capacity of multiple screw realizations following a Markov chain Monte Carlo approach. The axial capacity of the screw is obtained from nonlinear FE push-in simulations assuming an initial screw geometry corresponding to the first buckling mode with maximum amplitude expressed as a fraction of the screw length. The simulated data calibrate the imperfection coefficients for several defect amplitudes. Additionally, the authors estimated the uncertainty factor of the corresponding design equation for possible standard implementation.

In conclusion, it must be remarked that the experimental validation of the proposed model is impaired by the exiguous number of test

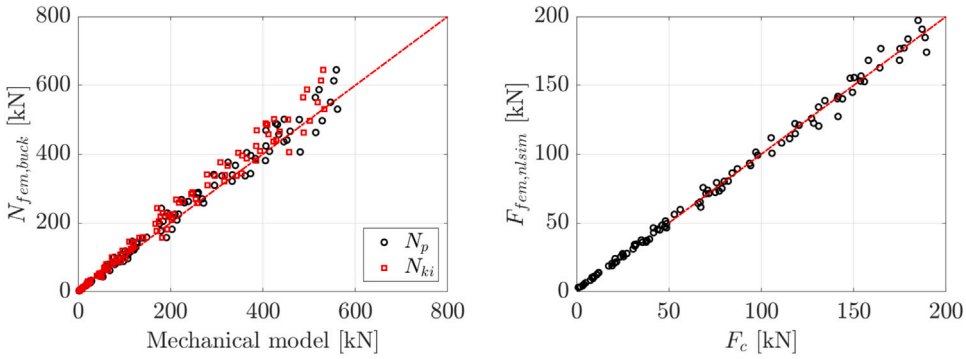

Fig. 15. (a) FE predictions of the theoretical buckling load vs the estimations using Eq. (6), and Eq. (17). (b) FE predictions of the axial capacity using N_p in Eq. (17) and the imperfection coefficients in Table 4.

repetitions and screw types. A few tests have been carried out to develop and validate the mathematical and FE models. Nonetheless, more extended experimental campaigns are needed to provide a solid empirical foundation for the proposed mechanical model.

CRediT authorship contribution statement

Angelo Aloisio: Conceptualization, Methodology, Experimental data analysis, Validation, Formal analysis, Numerical simulations, Investigation, Data curation, Writing – original draft, Writing and editing, Visualization, Supervision. **Yuri De Santis:** Conceptualization, Numerical simulations, Experimental data analysis, Validation, Formal analysis, Numerical simulations, Investigation, Data curation, Writing – original draft, Writing and editing, Visualization. **Matteo Pelliciari:** Conceptualization, Methodology, Formal analysis, Investigation, Writing – original draft, Writing and editing. **Marco Martino Rosso:** Numerical simulations, Investigation, Data curation. **Massimo Fragiacomo:** Visualization, Supervision. **Roberto Tomasi:** Experimental tests, Experimental data analysis, Validation, Formal analysis, Investigation, Resources, Data curation, Writing – original draft, Writing and editing, Visualization, Supervision.

Declaration of competing interest

The authors declare that they have no known competing financial interests or personal relationships that could have appeared to influence the work reported in this paper.

Data availability

Data will be made available on request.

Acknowledgements

The authors acknowledge Mathias Bech (Rothoblaas), Harald Liven (Moelven) and Peter Engström-Øren (SFS) for providing the material. Roar Økseter, Scott Brenna, Frode Anker Røsstad (NMBU) and the master thesis students Eldbjørg Aaraas Hånde and Kari Ryen Thunberg are kindly acknowledged for their support during the experimental campaign.

Appendix A. Discussion on the approximations in N_{ki}

The following discusses the buckling formulations' limitations for N_{ki}.

A.1. Shape of the buckling mode and boundary conditions

The theoretical buckling load of a Winkler beam, expressed by Eq. (6) , was derived by assuming the following buckled shape [35]:

$$v(x) = c \sin\left(\frac{m\pi x}{l_r}\right) \tag{A.1}$$

Following the energy method, the critical value of the load can be found by minimizing the deformation energy [35],

$$\Delta T = \Delta U_1 + \Delta U_2 \tag{A.2}$$

where Δ_T is the work done by the external forces, ΔU_1 is the internal strain energy associated with the bending, and ΔU_2 is the internal strain energy associated with the subgrade deformation.

This expression can be rewritten as a function of the buckled shape:

$$\frac{N}{2}\int_0^{l_r} v'(x)^2 dx = \frac{EI}{2}\int_0^{l_r} v''(x)^2 dx + \frac{c_h}{2}\int_0^{l_r} v^2(x) dx \tag{A.3}$$

where, in case of the sinusoidal expression of Eq. (A.1), the integrals can be written as:

$$\int_0^{l_r} v'(x)^2 dx = c^2\frac{m^2\pi^2}{2l_r} \quad \int_0^{l_r} v''(x)^2 dx = c^2\frac{m^4\pi^4}{2l_r^3} \quad \int_0^{l_r} v^2(x) dx = c^2\frac{l_r}{2} \tag{A.4}$$

Eq. (A.3) can be solved with respect to the applied load N, yielding the buckling load of a Winkler beam [35]:

$$N_w = \frac{\pi^2 EI}{l_r^2}\left(m^2 + \frac{c_h l_r^4}{m^2\pi^4 EI}\right) \tag{A.5}$$

where m is a positive integer number, indicating the number of half-waves of the sine function along the length of the bar. Note that a sine function with an integer number of half-waves fulfils the pinned–pinned boundary conditions.

The m associated with the first critical buckling load is determined by minimizing N_w in Eq. (A.5). This is done by setting the first derivative equal to zero:

$$m^4 - \frac{c_h l_r^4}{\pi^4 EI} = 0 \tag{A.6}$$

from which we obtain the expression

$$m = \frac{l_r}{\pi}\left(\frac{c_h}{EI}\right)^{1/4} \tag{A.7}$$

By substitution into Eq. (A.6), the critical load $N_{ki} = 2\sqrt{c_h EI}$ is derived.

In general, Eq. (A.7) does not give as a solution an integer number. Therefore, the expression of N_{ki} is associated with an inconsistent buckled mode that violates the boundary conditions, being m a real

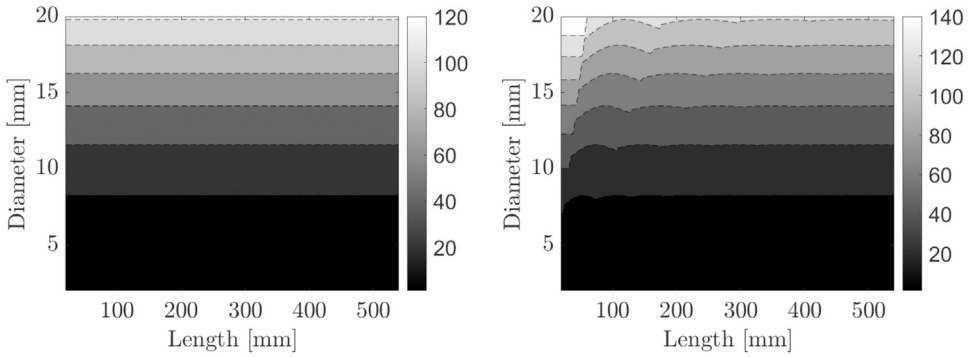

Fig. A.16. Contour plot of the axial resistance using Eq. (6) (a) and Eq. (A.5) (b) for the prediction of the theoretical buckling load.

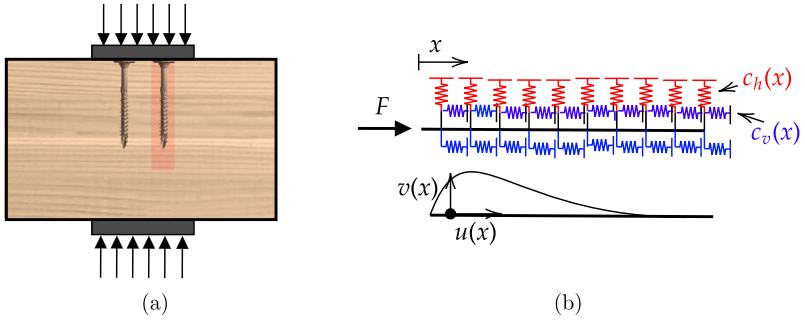

Fig. A.17. (a) Illustration of the load application from the steel plate in CPG problems; (b) Mathematical model of the screw under axial forces.

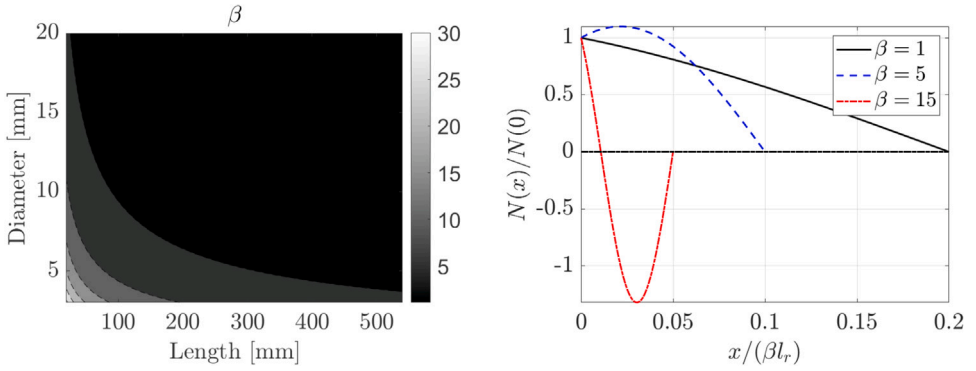

Fig. A.18. Contour plot of $\beta = c_v/EA$ and of the variation of the adimensional axial force in Eq. (A.11).

number instead of a positive integer number. Strictly speaking, its value should be determined as the closest integer (lower or greater) that provides the minimum value for N_w. Nevertheless, as reported in [53], the gap between the exact value of N_w and the approximation N_{ki} decreases with increasing values of m. Hence, especially for slender beams such as the screws, the difference between the two predictions can be neglected.

The authors calculated the values of the axial resistance and buckling load as a function of the diameter and threaded length of the screw using Eqs. (6) and (A.5). Fig. A.16 shows the contour plot of the axial resistance using Eq. (6) (a) and Eq. (A.5) (b) for the prediction of the theoretical buckling load.

The comparison between Figs. A.16(a) and (b) proves that the difference between N_w and N_{ki} is negligible.

A.2. Notes on the effect of a variable axial force

Another relevant approximation of Eqs. (6) and (A.5) is the assumption of a constant axial force along the screw. However, this is not true since only the head of the screw is directly loaded, while the tip cannot be in equilibrium with axial forces (Fig. A.17). Therefore, the axial force decreases along the screw length. This is also evident from the observed failure mode, where the deformation is concentrated at the screw head, where the axial force is higher.

However, as noted by Bejtka [4], a rigorous mathematical formulation for the buckling of screws is too demanding in complexity and computational effort. Therefore, Bejtka, acknowledging the fallacy of Eq. (A.5), replaced Eq. (6) with the buckling load from finite element analyses in Ansys. The researcher compiled several tables as a function of the diameter and the length, where intermediate values can be estimated with linear interpolation. Despite the merit of this study, tables of values are often difficult to handle, and a closed-form expression for the buckling load should be preferred. Therefore, despite all limitations, the EC5 proposal adopts Eq. (6) rather than tabular values.

In summary, the main limitations of the investigation of Bejtka are the following:

- The author does not consider a screw length higher than 240 mm. However, screws can be longer than that. Furthermore, instability

problems often slip common sense and the suitability of linear interpolations. The complexity of these problems demands the exploration of all the parameter domains to assess the presence of unique regions where the solution could be different than expected from inter and extrapolation.

- Using tabular values is not suitable for standard implementation.

Therefore, the analysis of Bejtka must allow for properly evaluating the error associated with using Eq. (6) due to the reduced number of values reported in the table and the limited extent of the domain.

The actual trend of the axial force can be approximately estimated from the following differential equation describing the axial equilibrium of the screw:

$$u''(x) + \beta^2 u(x) = 0; \quad \beta = \sqrt{\frac{c_v}{EA}} \tag{A.8}$$

where $u(x)$ is the axial displacement, c_v is the vertical stiffness of the elastic subgrade, and EA is the axial stiffness. The general solution is

$$u(x) = c_1 \sin \beta x + c_2 \cos \beta x \tag{A.9}$$

The boundary value problem can be solved by imposing the following boundary conditions:

$$EAu'(0) = F; \quad EAu'(l_r) = 0 \tag{A.10}$$

The expression for the axial force as a function of x is:

$$N(x) = F\left(\cos \beta x - \cot \beta l_r \sin \beta x\right) \tag{A.11}$$

The accuracy of $N(x)$ and consequently of β mostly depends on c_v, which possesses the primary source of uncertainty. As written in the introduction, multiple expressions exist for the axial capacity of the screw. For instance, Bejtka [4] proposed the following empirical regression for c_v, labelled $c_{v,exp}$.

$$c_{v,exp} = 234 \frac{(\rho d)^{0.2}}{l_r^{0.6}} \tag{A.12}$$

The applicability of Eq. (A.12) in Eq. (A.11) is further examined in Appendix B.

Fig. A.18 shows the contour plot of β for different diameters and screw lengths using Eq. (A.12), Young's modulus for steel equal to 210 GPa and wood density equal to 400 kg/m^3. Parameter β varies between almost 5 and 30 for short screws with a small diameter. In all practical cases, β is lower than 5. These values are associated with an almost linear distribution of N. Conversely, values higher than ten significantly increment the axial force compared to the one at $x = 0$. It must be remarked that in all design circumstances, the trend of $N(x)$ is almost linear.

In light of the above, a rigorous buckling model should consider the variation of the axial force along the screw axis. However, this problem cannot be treated analytically [59–63]. In fact, there are still no closed-form solutions available in the literature. Hence, in the present work, we propose that the effect of the variation of $N(x)$ is directly considered in the deformed shape of the screw by assuming a damped sine as buckled configuration (see Section 4).

In other words, the main effect of the concentration of axial force at the head of the screw is to produce a buckling mode well approximated by a damped sine. In this way, the axial contribution to the strain energy can still be neglected, and the effect of the variation of axial force is already included in the deformed shape. Hence, in Section 4, the axial force in the energy method is kept constant.

The axial stiffness of the elastic medium (c_v) was obtained by Bejtka [4] by dividing the axial stiffness of the screw (K_{ax}) by the length of the screw (l_r) as follows:

$$K_{ax} = c_{v,exp} \cdot l_r = \frac{F}{u(l_r)} \tag{A.13}$$

where K_{ax} was derived experimentally by dividing the applied force at the tip (F) and the measured displacement at the head $u(l_r)$, assuming

Table A.11
Comparison between pinned-head and free-head buckling and failure load according to finite element models.

Config.	$N_{fem,buck}$ [kN]	$N_{fem,buck}$	ratio	$F_{fem,NLSIM}$	$F_{fem,NLSIM}$ [kN]	ratio
Boundary	pinned	free		pinned	free	
T-7.0–160	73.0	30.6	0.42	23.3	19.7	0.85
T-8.2–160	109.7	44.1	0.40	32.3	29.8	0.92
T-8.0–160	99.5	41.1	0.41	30.7	26.9	0.88
T-8.0–180	97.3	40.7	0.42	30.5	25.5	0.84
T-8.0–200	95.6	40.5	0.42	30.3	25.1	0.83
T-8.0–300	90.6	39.7	0.44	29.2	22.9	0.78
T-8.0–340	89.4	39.5	0.44	28.8	22.1	0.77
T-9.0–440	113.7	50.4	0.44	35.9	27.0	0.75

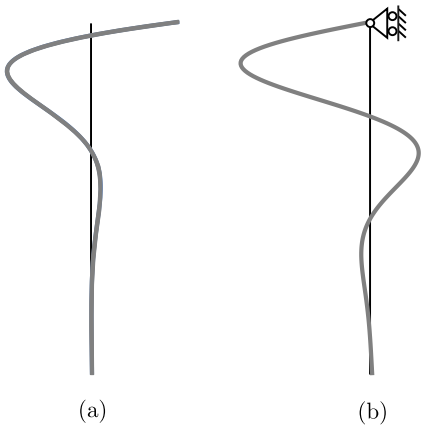

Fig. A.19. Buckling shapes of (a) free-head screw and (b) hinged-head screw.

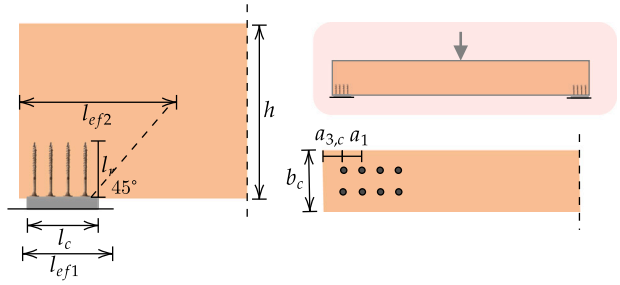

Fig. B.20. Illustration of the design application and the notation.

$x = 0$ at the load application point. Eq. (A.11) reveals that the axial force is not constant (see Eq. (A.11)). Rigorously the stiffness of the screw, obtained by dividing the applied force by the measured displacement at the head, can be written as:

$$K_{ax} = \frac{F}{u(l_r)} = \beta EA \sin(\beta l_r) \tag{A.14}$$

The values of c_v were experimentally derived in [42] with short screws. Thus, the following approximation holds in (A.14), $\sin(\beta l_r) \approx \beta l_r$. Accordingly, the K_{ax} can be approximated by:

$$K_{ax} \approx \beta^2 l_r EA = c_v l_r \tag{A.15}$$

Therefore, by equalling Eq. (A.13) with Eq. (A.15), the following holds $c_v \approx c_{v,exp}$. It must be remarked that this approximation can be considered valid only if $c_{v,exp}$ is derived experimentally with short screws, where $\sin(\beta l_r) \approx \beta l_r$. Then the value of $c_{v,exp}$ obtained for shorter screws can also be used in the analysis when dealing with longer screws.

Table B.12
Calculation example of the capacity of a timber member under compression perpendicular to the grain with screw reinforcement. The table sections on the buckling resistance and design model have two parts, one for the prEN 1995 1.1 model and the one proposed in this paper.

Input data							
Timber GL30c		Screw VGZ 7.0 × 160		k_{pr}	1.5	n [mm]	4
$f_{c,90,k}$ [Mpa]	2.5	d [mm]	8	b_c [mm]	140	n_0	2
h [mm]	400	d_1 [mm]	4.6	l_c [mm]	180	α	90
b [mm]	140	l_r [mm]	300	a_1 [mm]	70		
ρ_k [kg/m^3]	390	$f_{y,k}$ [mm]	1200	a_{3c} [mm]	365		
Withdrawal resistance				Buckling resistance			
k_w	1	$f_{w,k}$ [MPa]	4.65	PrEN 1995 1.1		Proposed model	
k_{mat}	1	$F_{w,k}$ [kN]	35.05	$N_{pl,k}$	19.94	$N_{pl,k}$	19.93
k_p	1.1			c_h	111.54	c_h	111.54
Design model				$N_{ki,k}$	22.68	$N_{ki,k}$	53.08
PrEN 1995 1.1		Proposed model		λ_k	0.938	λ_k	0.613
Min($F_{c,k}$, $F_{w,k}$)	13.58	Min($F_{c,k}$, $F_{w,k}$)	21.38	α_g	0.49	α_g	0.16
$l_{ef,1}$ [mm]	240	$l_{ef,1}$ [mm]	240	κ	1.12	κ	0.72
$l_{ef,2}$ [mm]	670	$l_{ef,1}$ [mm]	670	κ_c	0.58	κ_c	0.91
A_1 [kN]	180.30	A_1 [kN]	211.51	F_{ck}	13.58	F_{ck}	21.38
A_2 [kN]	234.50	A_2 [kN]	234.50				
F_k [kN]	180.30	F_k [kN]	211.51				

A.3. Note on the choice of the boundary conditions

The buckling load reported in the EC5 draft is $N_{ki} = \sqrt{c_h EI}$, which is precisely half of the expression of Eq. (6) . As observed by Bejtka [25], this expression approximately corresponds to the theoretical buckling load for elastic beams with free ends embedded in an elastic foundation, which is in good agreement with the FE simulations where these boundary conditions are adopted. This leads to almost half of the buckling load in Eq. (6) , as shown in Table A.11.

However, in many practical circumstances, when friction forces arise between the screw and the steel plate, the lateral displacement of the head of the screw can be considered negligible (also in agreement with the experimental evidence observed in the Torx test). In this case, assuming a constant vertical load, the theoretical buckling load for double pinned elastic beams embedded in an elastic foundation is $N_{ki} = 2\sqrt{c_h EI}$, which is the one reported in Eq. (6) . The buckling shapes associated with these two boundary conditions are compared in Fig. A.19. It is worth reminding, according to [35], that the theoretical solution of Eq. (6) assumes a sinusoidal buckling shape, while in this paper, the theoretical expression of Eq. (17) is derived with a buckling shape of the form of Fig. A.19(b), coherently with the experimental evidence.

Appendix B. Application

The proposed formulation has been applied to a typical design problem involving the buckling capacity of the screw, i.e. the resistance of a timber member with screw reinforcement under compression perpendicular to the grain. It can be the case of a simply-supported beam, as illustrated in Fig. B.20. The design follows the PrEN 1995 1.1 using the equations below.

$$F_k = \min \begin{cases} A_1 = k_{pr} \cdot b_c \cdot l_{ef,1} \cdot f_{c,90,k} + n \cdot min\{F_{w,k}, F_{c,k}\}, \\ A_2 = b \cdot l_{ef,2} \cdot f_{c,90,k} \end{cases}, \tag{B.1}$$

$$l_{ef,1} = l_c + \min\{30\ \text{mm}, l_c\} + \min\{30\ \text{mm}, l_c, l_e\} \tag{B.2}$$

$$l_{ef,2} = l_r + (n_0 - 1) \cdot a_1 + \min\{l_r, a_{3,c}\} \tag{B.3}$$

The definition of all symbols is given in the initial list of symbols and notation. In place of the standard buckling model, the authors also used the proposed one to understand the practical consequences related to its use. Two important aspects need to be remarked: (1) the proposed equation has not been validated against the experimental capacity of multiple screws loaded in compression. Further investigations are required to understand the accurate modelling of the so-called group effect. (2) The proposed model assumes the additivity between the timber and screw capacity contributions. This aspect has been recently questioned in [64] and needs further investigations.

Table B.12 reports the results of the calculations. It is organized into four sections, the input data, two sections dedicated to predicting the withdrawal and buckling resistance of the screw, and the last section to the model capacity. Based on this example, the reader can calculate the capacity of the tested samples using geometric and material parameters.

This design case proves that the model in PrEN 1995 1.1 might lead to a consistent underestimation of the capacity by approximately 17%.

References

[1] H. Blass, J. Ehlbeck, H. Kreuzinger, G. Steck, Erläuterungen zu DIN 1052: 2004-08: Entwurf, Berechnung und Bemessung von Holzbauwerken; Inkl, 2004.
[2] Eurocode 5: Design of timber structures - Part 1-1: General - Common rules and rules for buildings, 2010, NS-EN 1995-1-1:2004+A1:2008+NA:2010.
[3] A. Leijten, S. Franke, P. Quenneville, R. Gupta, Bearing strength capacity of continuous supported timber beams: Unified approach for test methods and structural design codes, J. Struct. Eng. 138 (2) (2012) 266–272.
[4] I. Bejtka, Verstärkung von bauteilen aus holz mit vollgewindeschrauben, KIT Scientific Publishing, 2005.
[5] M. Piazza, R. Modena, R. Tomasi, Strutture in legno. Materiale, calcolo e progetto secondo le nuove normative europee, Hoepli Editore, 2005.
[6] G. Pirnbacher, G. Schickhofer, Schrauben im vergleich-eine empirische betrachtung, in: GraHFT'07, Vol. 6, 2007, cited by 6.
[7] P. Dietsch, R. Brandner, Self-tapping screws and threaded rods as reinforcement for structural timber elements–a state-of-the-art report, Constr. Build. Mater. 97 (2015) 78–89.
[8] F. Colling, Holzbau-grundlagen und bemessungshilfen. 2. auflage, in: Holzbau-Grundlagen und Bemessungshilfen, 2008.
[9] F. Boggian, A. Aloisio, R. Tomasi, Experimental and analytical study of friction connection for seismic retrofit with cross-laminated timber (clt) panels, Earthq. Eng. Struct. Dyn. 51 (14) (2022) 3304–3326.
[10] H. Kreuzinger, Holzbau, in: Handbuch für Bauingenieure, 2002.
[11] R. Tomasi, A. Crosatti, M. Piazza, Theoretical and experimental analysis of timber-to-timber joints connected with inclined screws, Constr. Build. Mater. 24 (9) (2010) 1560–1571.
[12] R. Tomasi, A. Aloisio, E.A. Hånde, K.R. Thunberg, E. Ussher, Experimental investigation on screw reinforcement of timber members under compression perpendicular to the grain, Eng. Struct. 275 (2023) 115163.
[13] G. Schiro, I. Giongo, W. Sebastian, D. Riccadonna, M. Piazza, Testing of timber-to-timber screw-connections in hybrid configurations, Constr. Build. Mater. 171 (2018) 170–186.
[14] H. Kreuzinger, Platten, Platten, scheiben und schalen - ein berechnungsmodell für gängige statikprogramme, Bauen Mit Holz 1 (1) (1999) 34–39.
[15] H. Kreuzinger, Verbundkonstruktionen, in: Holzbaukalender 2002, 2001, pp. 598–621.
[16] D.E. 1-1/NA, Norwegian national annex - Nationally determined parameters - Eurocode 5: Design of timber structures - Part 1-1: General - Common rules and rules for buildings, 2010.

[17] S. Aicher, L. Höfflin, Glulam beams with round holes-a comparison of different design approaches vs. test data, cib-w18/35-12-1, in: Proceedings of the International Council for Research and Innovation in Building and Construction, Working Commission W18-timber Structures, 2002.
[18] S. Aicher, L. Höfflin, Design of rectangular holes in glulam beams, Otto-Graf-J. 14 (2003) 211–229.
[19] H. Kolb, A. Epple, Verstärkungen von Durchbrochenen Brettschichtholzbindern, Schlussbericht Zum Forschungsvorhaben I.4-34810, 1985.
[20] S. Aicher, L. Höfflin, H.-W. Reinhardt, Round holes in members made of glued laminated timber. part 2: Load capacity and design [runde durchbrüche in biegeträgern aus brettschichtholz teil 2: Tragfähigkeit und bemessung], Bautechnik 84 (12) (2007) 867–880.
[21] S. Aicher, L. Höfflin, Glulam beams with holes reinforced by steel bars, glulam beams with holes reinforced with steel bars, 2009.
[22] S. Aicher, Glulam beams with internally and externally reinforced holes - test, detailing and design, in: International Council for Research and Innovation in Building and Construction, Working Commission W18 - Timber Structures, Alghero, Italy, 2011, pp. 1–13.
[23] P. Dietsch, S. Rodemeier, H. Blaß, Transmission of perpendicular to grain forces using self-tapping screws, in: International Network on Timber Engineering Research INTER, Meeting 6, 2019.
[24] I. Bejtka, J. Blass H., Self-tapping screws as reinforcements in connections with dowel-type fasteners, cib-w18/38-7-4, in: Proceedings of the International Council for Research and Innovation in Building and Construction, Working Commission W18-Timber Structures, Meeting 38, Karlsruhe, Germany, 2005.
[25] I. Bejtka, J. Blass H., Self-tapping screws as reinforcements in beam supports, cib-w18/39-7-2, in: Proceedings of the International Council for Research and Innovation in Building and Construction, Working Commission W18-Timber Structures, Meeting 39, Florence, Italy, 2006.
[26] H. Blass, G. Steck, Querzugverstärkungen von holzbauteilen: Teil 1 - teil 3, 101, 3, 1999, pp. 42–46.
[27] H. Blass, I. Bejtka, Querzugverstärkungen in Gefährdeten Bereichen mit Selbstbohrenden Holzschrauben, 2003 (in German).
[28] E. Suenson, Zulässiger druck auf querholz, Holz als Roh-und Werkstoff 1 (6) (1938) 213–216.
[29] B. Standard, Eurocode 3—design of steel structures—, BS EN 1993-1, 1, 2005, p. 2006.
[30] H.G. Poulos, E.H. Davis, et al., Pile Foundation Analysis and Design, Vol. 397, Wiley New York, 1980.
[31] H. Granholm, On the Elastic Stability of Piles Surrounded By a Supporting Medium, Vol. 89, Svenska Bokhandelscentralen A.-B, 1929.
[32] M. Hetenyi, Beams on elastic foundation, 1946, cited by 1456.
[33] M. Eisenberger, D. Yankelevsky, Exact stiffness matrix for beams on elastic foundation, Comput. Struct. 21 (6) (1985) 1355–1359, cited by 78.
[34] R. West, M. Pavlović, A fast iterative algorithm for eigenvalue determination, Comput. Struct. 63 (4) (1997) 749–758.
[35] S.P. Timoshenko, J.M. Gere, Theory of elastic systems, 1961.
[36] K. Terzaghi, Evaluation of coefficients of subgrade reaction, Geotechnique 5 (4) (1955) 297–326, cited by 517.
[37] Design of laterally loaded piles, vol. 103, 1984, cited by 1.
[38] R. West, Modal clustering in the vibration of beams partially embedded in a Winkler foundation, 1991, cited by 5.
[39] R. Cucuzza, G. Devillanova, A. Aloisio, M.M. Rosso, G.C. Marano, Analytical solutions for piles' lateral deformations: The nonlinear stiffness case, Int. J. Mech. Sci. 229 (2022) 107505.
[40] M.E. Heelis, R.P. West, et al., The stability of uniform-friction piles inhomogeneous and non-homogeneous elastic foundations, Int. J. Solids Struct. 36 (22) (1999) 3277–3292.
[41] A.D. Kerr, On the buckling of slender piles, Soils Found. 28 (2) (1988) 144–148.
[42] H.J. Blaß, I. Bejtka, T. Uibel, Tragfähigkeit von Verbindungen mit selbstbohrenden Holzschrauben mit Vollgewinde, vol. 4, 2006.
[43] A. Ringhofer, M. Grabner, R. Brandner, G. Schickhofer, Sgsc 3.2.1-1-prüftechnische ermittlung des tragverhaltens der einzelschraube in der bsp-schmalfläche, Internal Research Report, Holz.Bau Forschungs Gmbh, Institute of Timber Engineering and Wood Technology, 2013.
[44] H. Stamatopoulos, K.A. Malo, On strength and stiffness of screwed-in threaded rods embedded in softwood, Constr. Build. Mater. 261 (2020) 119999.
[45] J. Ehlbeck, R. Görlacher, H. Werner, Determination of perpendicular-to-the-grain tensile stresses in joints with dowel-type-fasteners, in: Proceedings of CIB-W18, 1989.
[46] H. Kolb, P. Frech, Untersuchungen an durchbrochenen bindern aus brettschichtholz [untersuchungen an durchbrochenen bindern aus brettschichtholz], Eur. J. Wood Wood Ind. 35 (4) (1977) 125–134.
[47] Eurocode 5. design of timber structures. bridges, Eurocode 5: Design of timber structures - part 1-1: General - Common rules and rules for buildings, 2004, cited by 841.
[48] Y. De Santis, M. Fragiacomo, Timber-to-timber and steel-to-timber screw connections: Derivation of the slip modulus via beam on elastic foundation model, Eng. Struct. 244 (2021) 112798.
[49] M.A.H. Mirdad, A. Jucutan, R. Khan, J. Niederwestberg, Y.H. Chui, Embedment and withdrawal stiffness predictions of self-tapping screws in timber, Constr. Build. Mater. 345 (2022) 128394.
[50] R. Jockwer, A. Frangi, R. Steiger, E. Serrano, Enhanced design approach for reinforced notched beams, cib-w18/46-6-1, in: Proceedings of the International Council for Research and Innovation in Building and Construction, Working Commission W18-Timber Structures, 2013.
[51] H.M. Kattan, Those who fail to learn from history are doomed to repeat it, in: Agile Processes in Software Engineering and Extreme Programming: Poster Presented in the 18th International Conference on Agile Software Development, xp 2017, Cologne, germany, 2017.
[52] G. Ballio, F.M. Mazzolani, Theory and Design of Steel Structures, Taylor & Francis, 1983.
[53] O. Belluzzi, Scienza delle Costruzioni, Vol. 4, Zanichelli, 1982.
[54] C.P. Robert, G. Casella, Monte Carlo Statistical Methods, Vol. 2, Springer, 1999.
[55] D. Bigoni, Nonlinear Solid Mechanics: Bifurcation Theory and Material Instability, Cambridge University Press, 2012.
[56] A. Ringhofer, M. Augustin, G. Schickhofer, Basic steel properties of self-tapping timber screws exposed to cyclic axial loading, Constr. Build. Mater. 211 (2019) 207–216.
[57] P. Niebuhr, M. Sieder, High-cycle fatigue behavior of a self-tapping timber screw under axial tensile loading, J. Fail. Anal. Prev. 20 (4) (2020) 580–589.
[58] A.Y. Al-Attraqchi, M.J. Hashemi, R. Al-Mahaidi, Hybrid simulation of bridges constructed with concrete-filled steel tube columns subjected to horizontal and vertical ground motions, Bull. Earthq. Eng. 18 (9) (2020) 4453–4480.
[59] N. Tullini, A. Tralli, D. Baraldi, Stability of slender beams and frames resting on 2D elastic half-space, Arch. Appl. Mech. 83 (3) (2013) 467–482.
[60] N. Tullini, A. Tralli, D. Baraldi, Buckling of timoshenko beams in frictionless contact with an elastic half-plane, J. Eng. Mech. 139 (7) (2013) 824–831.
[61] F.O. Falope, L. Lanzoni, E. Radi, Buckling of a timoshenko beam bonded to an elastic half-plane: Effects of sharp and smooth beam edges, Int. J. Solids Struct. 185 (2020) 222–239.
[62] M. Eisenberger, Buckling loads for variable cross-section members with variable axial forces, Int. J. Solids Struct. 27 (2) (1991) 135–143.
[63] D. Hui, Postbuckling behavior of infinite beams on elastic foundations using Koiter's improved theory, Int. J. Non-Linear Mech. 23 (2) (1988) 113–123.
[64] A. Aloisio, E. Ussher, M. Fragiacomo, R. Tomasi, Capacity models for timber under compression perpendicular to grain with screw reinforcement, Eur. J. Wood Wood Prod. (2023) 1–22.